Observational effects of the early episodically dominating dark energy

Chan-Gyung Park[1], Jae-heon Lee[2], Jai-chan Hwang[2], and Hyerim Noh[3]
[1]*Division of Science Education and Institute of Fusion Science, Chonbuk National University, Jeonju 561-756, Republic of Korea*
[2]*Department of Astronomy and Atmospheric Sciences, Kyungpook National University, Daegu 702-701, Republic of Korea*
[3]*Korea Astronomy and Space Science Institute, Daejeon 305-348, Republic of Korea*
(Dated: March 5, 2015)

We investigate observational consequences of the early episodically dominating dark energy on the evolution of cosmological structures. For this aim, we introduce the minimally coupled scalar field dark energy model with the Albrecht-Skordis potential which allows a sudden ephemeral domination of dark energy component during the radiation or early matter era. The conventional cosmological parameters in the presence of such an early dark energy are constrained with WMAP and Planck cosmic microwave background radiation data including other external data sets. It is shown that in the presence of such an early dark energy the estimated cosmological parameters can deviate substantially from the currently known ΛCDM-based parameters, with best-fit values differing by several percents for WMAP and by a percent level for Planck data. For the latter case, only a limited amount of dark energy with episodic nature is allowed since the Planck data strongly favors the ΛCDM model. Compared with the conventional dark energy model, the early dark energy dominating near radiation-matter equality or at the early matter era results in the shorter cosmic age or the presence of tensor-type perturbation, respectively. Our analysis demonstrates that the alternative cosmological parameter estimation is allowed based on the same observations even in Einstein's gravity.

PACS numbers: 98.80.-k, 95.36.+x

arXiv:1407.1512v2 [astro-ph.CO] 4 Mar 2015

I. INTRODUCTION

The *precision cosmology* is often mentioned in present day cosmology in the sense that the model parameters are constrained with a few percent precision level [1, 2]. The future projects for cosmological observations also forecast the sub-percent level parameter estimation in the optimistic situation (e.g., see [3] for Euclid project). However, most of considerations for the observational precision rely on the concordance cosmology based on the ΛCDM model with the cosmological constant Λ as the dark energy, the cold dark matter (CDM) as the dominant dark matter, and the initial density and gravitational wave power spectra provided by the inflation era in the early universe. For the Λ, the effect of dark energy on the evolution of universe at the early epoch is negligible or small. Even in the dynamical dark energy models, attentions have been paid on the late-time behavior of the dark energy that starts to dominate the matter component only at very recent epoch, $z \lesssim 1$.

As soon as we introduce a dynamical dark energy, its prehistory could become important [4], and it is certainly allowed that the dark energy may dominate at some earlier epoch without violating observational constraints, but with differing cosmological parameter estimations. In order to demonstrate such possibilities of alternative cosmological parameter estimations in Einstein's gravity, here we would like to investigate one such a model based on a known dark energy model proposed in the literature as an example. By introducing an early dark energy (EDE) which becomes ephemerally dominant in the early cosmological era, we will show that there exists room for alternative cosmological parameter estimation based on the same cosmological observations.

A simple *fluid* model of EDE is known in the literature which accommodates the scaling behavior of dark energy so that the dark energy density parameter is constant before the onset of the late-time acceleration [5]. Observational constraints on the fluid-based EDE model were given by several groups using the cosmic microwave background radiation (CMB), baryon acoustic oscillation (BAO), type Ia supernovae (SNIa), Lyman-α forest, and Hubble constant data [5–11]. The recent constraint on the EDE density parameter from the Planck observation is $\Omega_e \lesssim 0.01$ (95% confidence limit) [2]. There are also studies on the transient acceleration models where the universe might be decelerated in the near future [12, 13].

Here, we consider an early episodically (or ephemerally) dominating dark energy model based on the scalar field which transiently becomes important in the radiation- or early matter-dominated era before the onset of the late-time acceleration. Our aim is to investigate the observational effects and the consequent cosmological parameter estimations based on the observationally indistinguishable altered dark energy models. Our field theory based model can accommodate the purely scaling behavior of dark energy component and is free from the ambiguity seen in the fluid-based EDE model. For the latter model, the behavior of the dark energy perturbation variables strongly depends on the definition of sound speed and the method of dealing with the dynamical property of the dark energy clustering.

This paper is organized as follows. Section II describes the scalar-field-based EDE model adopted here. We

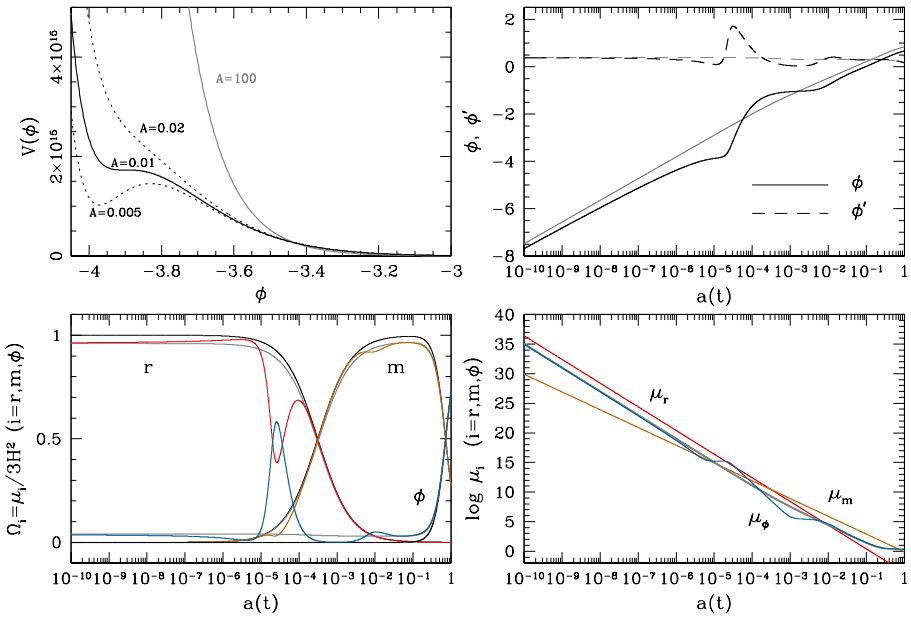

FIG. 1: Top-left: A close-up picture of the scalar field potential [Eq. (1) in unit of H_0^2] in an EDE model with $\phi_0 = -4$, $A = 0.01$, and $\lambda = 10$ (black solid curve). The cases for $A = 0.005$ and 0.02 are shown as dotted curves while that of SDE model ($A = 100$, $\phi_0 = -3$) as a gray curve with the potential amplitude suppressed by a factor of 300 for ease of display. Top-right: Evolution of ϕ and its time-derivative $\phi' = d\phi/d\ln a$ in the EDE (black) and the SDE (gray curve) models as a function of the scale factor $a(t)$ normalized to unity at present. Bottom: Evolution of background density parameters (Ω_i) and energy densities (μ_i) of radiation ($i = r$, red), matter (m, brown), and scalar field (ϕ, blue curves) in the EDE model. The gray and black curves indicate the evolutions for the SDE and fiducial ΛCDM models, respectively.

present the numerical calculations of background evolution of the EDE model and provide the empirical method of obtaining the initial conditions of the scalar field variables. In Sec. III, we show how matter and CMB power spectra are affected by the presence of EDE, and constrain the conventional cosmological parameters for selected EDE models using the recent cosmological observations. The summary and conclusion are given in Sec. IV. Throughout this paper, we set $c \equiv 1 \equiv 8\pi G$.

II. EARLY EPISODICALLY DOMINATING DARK ENERGY MODEL

To mimic the episodic behavior of dark energy we consider a minimally coupled scalar field with the potential

$$V(\phi) = V_0[(\phi - \phi_0)^2 + A]e^{-\lambda\phi} + V_1 e^{-\beta\phi}. \qquad (1)$$

The first term is known as the Albrecht-Skordis potential with two interesting points [14]: (i) it allows the *near* scaling evolution where the energy density of the scalar field scales with the dominant fluid density during the evolution, and (ii) it drives the accelerated expansion of the universe. It is known that both the permanent ($A\lambda^2 \lesssim 1$) and the ephemeral ($A\lambda^2 \gtrsim 1$) accelerations are possible depending on a choice of parameters A and λ [15]. The previous studies on the transient nature of dark energy with the Albrecht-Skordis potential were mainly focused on its recent transient behaviors [13, 16, 17]. On the other hand, here we consider a different case in which the transient dark energy domination occurs before the onset of the late-time acceleration that will be driven by the second term of Eq. (1) (see [18] for a similar work). For simplicity, we set $\beta = 0$ throughout this work. Thus, the parameter V_1 behaves as the cosmological constant Λ.

Figure 1 shows an example of evolution of our EDE model, where an extremely shallow local minimum was set by choosing $\phi_0 = -4$, $A = 0.01$ for $\lambda = 10$. The value of λ is related to the initial dark energy density parameter as $\Omega_{\phi i} = 4/\lambda^2$ during the radiation-dominated era and has been chosen to satisfy the big bang nucleosynthesis bound ($\Omega_{\phi i} < 0.045$) [16, 19]. In this case the scalar field starts to roll down the potential with scaling behavior, gets slower until it arrives at the local minimum, and then suddenly kicks and rolls rapidly down the potential out of the minimum. The rolling becomes slower as time goes by, and the dark energy acquires the scaling nature again because the field rolls down the potential which is effectively similar to the exponential one. We consider a special case with a large value of $A = 100$ ($\phi_0 = -3$; gray curves), which shows the effective scaling behavior without the episodic dark energy domination. Hereafter, we refer to such a model as the scaling dark energy (SDE) model.

We evolve a system of multiple components for radiation, matter, and a minimally coupled scalar field without

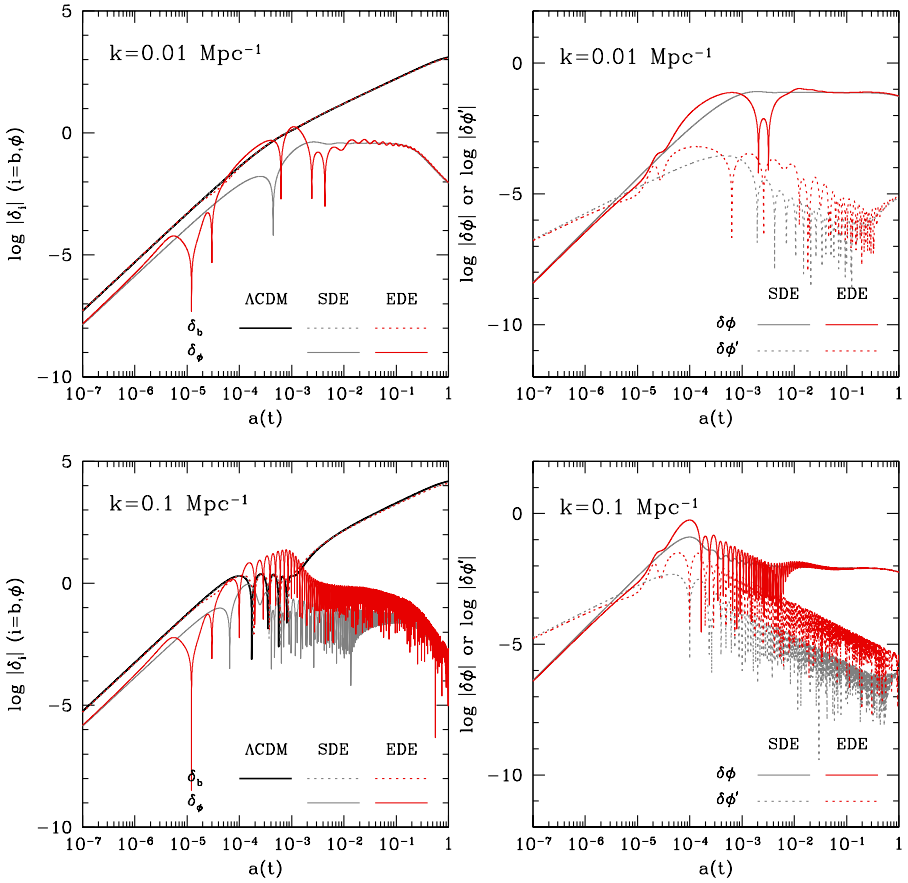

FIG. 2: Evolution of density perturbations of baryon (δ_b) and dark energy (δ_ϕ) components (left) and that of scalar field perturbation variables ($\delta\phi$ and $\delta\phi' = d\delta\phi/d\ln a$; right column) in the EDE model considered in Fig. 1 (red curves), for comoving wavenumbers $k = 0.01$ (top) and 0.1 Mpc^{-1} (bottom panels). As the temporal gauge condition, the CDM-comoving gauge (where the velocity of the cold dark matter vanishes) has been chosen. The gray and black curves indicate the evolutions for the SDE and fiducial ΛCDM models, respectively.

direct mutual interactions among the components. Our convention and the basic equations are summarized in Refs. [19, 20]. A set of initial conditions for the scalar field has been obtained with an empirical method to give the scaling behavior of dark energy. From the scaling evolution of the scalar field, we have energy density and pressure as

$$\mu_\phi \propto \mu_w, \quad p_\phi = w\mu_\phi, \tag{2}$$

where μ_w is the energy density of the dominant fluid with equation-of-state parameter w. Combining the time-derivatives of μ_ϕ and p_ϕ with the equation of motion for scalar field gives a relation

$$\phi' = -3(1+w)\frac{V}{V_{,\phi}}, \tag{3}$$

where a prime indicates a derivative with respect to $\ln a$. Next, at the initial epoch $a_i = 10^{-10}$ we choose a trial initial value of ϕ_i within a sufficiently wide interval of $\phi < \phi_0$, and obtain the initial condition for ϕ_i' using the above relation. From the scaling evolution of dark energy, we impose a condition that the second derivative ϕ'' should vanish at the initial stage (numerically $|\phi''| < 10^{-7}$; see the constant nature of ϕ' for SDE model; Fig. 1, top-right panel). By changing the value of ϕ_i using the bisection iteration technique we obtain very accurate initial conditions for ϕ and ϕ' within trials of about 30 times. For each background evolution with these initial conditions, the value of V_1 has been adjusted to satisfy the condition $H/H_0 = 1$ at the present epoch, where $H = \dot{a}/a$ is the Hubble parameter. During setting these initial conditions, we simply set $V_0/H_0^2 \equiv 1$. In the appendix, we present the initial conditions of background scalar field variables (ϕ_i, ϕ_i') together with the potential parameters of EDE (SDE) models considered in this paper.

For the scalar field perturbation variables, $\delta\phi$ and $\delta\phi'$, we have adopted the scaling initial conditions for the pure exponential potential case [19],

$$\delta\phi = \frac{3(1-w)}{(7+9w)\lambda}\delta_w, \quad \delta\phi' = 2\delta\phi \tag{4}$$

where $\delta_w \equiv \delta\mu_w/\mu_w \propto a^{1+3w}$ is the growing-mode so-

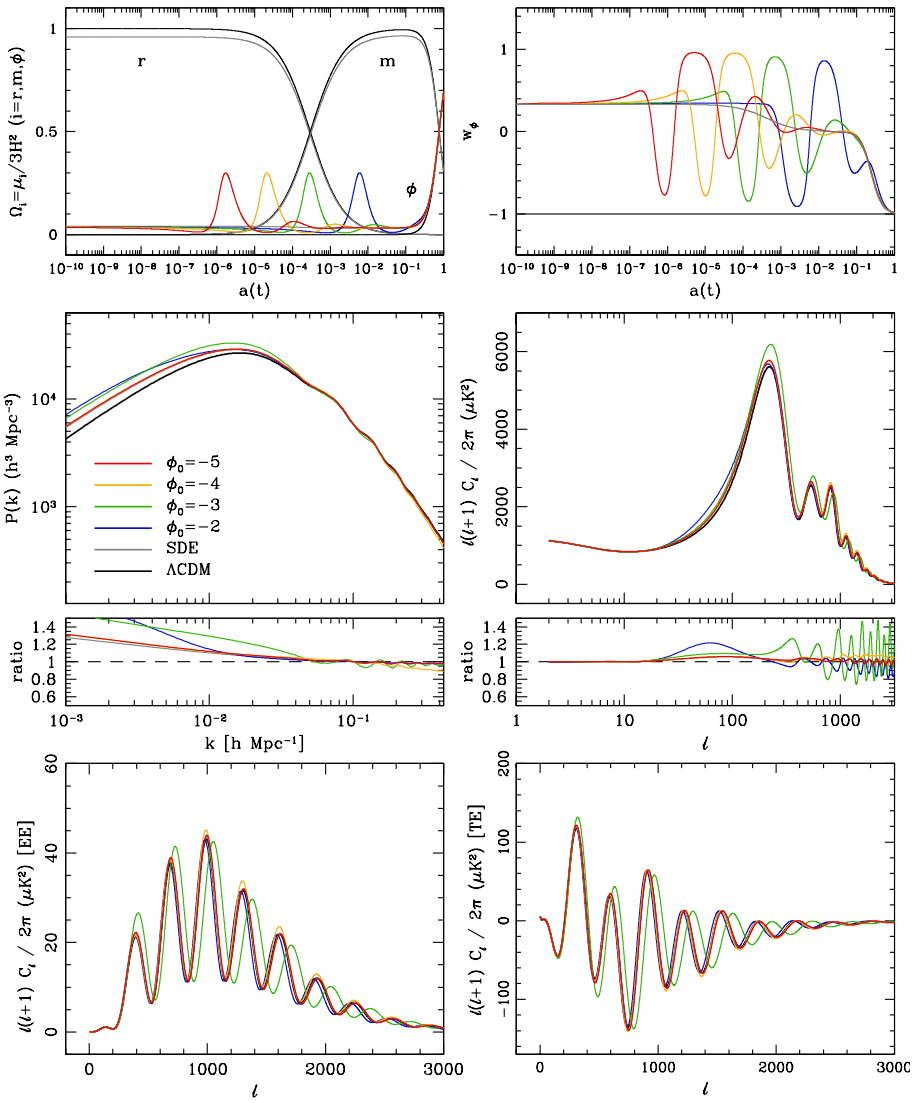

FIG. 3: Evolution of density parameters (Ω_i; $i = r,\ m,\ \phi$) and dark energy equation-of-state parameters (w_ϕ) (top), and power spectra of baryonic matter density (middle-left), and of CMB temperature anisotropy (middle-right) and polarization (bottom panels) in our EDE models with $\phi_0 = -5$ (red), -4 (yellow), -3 (green), -2 (blue curves). For each value of ϕ_0, A has been adjusted to give $\Omega_\phi = 0.3$ at the peak of early episodic domination of dark energy component. In all EDE models, we set $\lambda = 10$. Grey curves represent the results of scaling dark energy (SDE) model, and black curves those of the fiducial ΛCDM model. The matter power spectra are normalized to the ΛCDM model prediction at $k = 0.1\ h\mathrm{Mpc}^{-1}$, while the CMB anisotropy power spectra at $\ell = 10$. For matter and CMB temperature anisotropy power spectra, the ratio of EDE model power spectrum to ΛCDM prediction is also shown based on such a normalization.

lution of density perturbation variable for the dominant w-fluid. These initial conditions are valid to use because the background evolution of our EDE model shows very accurate scaling evolution in the early era. Although these are not the exact initial conditions, the actual evolution of perturbation variables shows a scaling behavior quite well.

Figure 2 shows evolution of density perturbations of baryon ($\delta_b = \delta\mu_b/\mu_b$) and scalar-field dark energy ($\delta_\phi = \delta\mu_\phi/\mu_\phi$) in the CDM-comoving gauge, together with that of scalar field perturbation variables ($\delta\phi$, $\delta\phi'$) at two different comoving scales ($k = 0.01,\ 0.1\ \mathrm{Mpc}^{-1}$) for the EDE model ($A = 0.01$, $\phi_0 = -4$, $\lambda = 10$) in Fig. 1. Note that the evolution of baryon density perturbations (red dotted) slows down during the episodic domination of dark energy (around $a \approx 3 \times 10^{-5}$), compared with the cases of ΛCDM (black solid) and SDE models (gray dotted curves; Fig. 2 left panels), and that the amplitude of dark energy perturbations becomes quite weaker during the recent epoch when the late-time acceleration is driven by the cosmological constant.

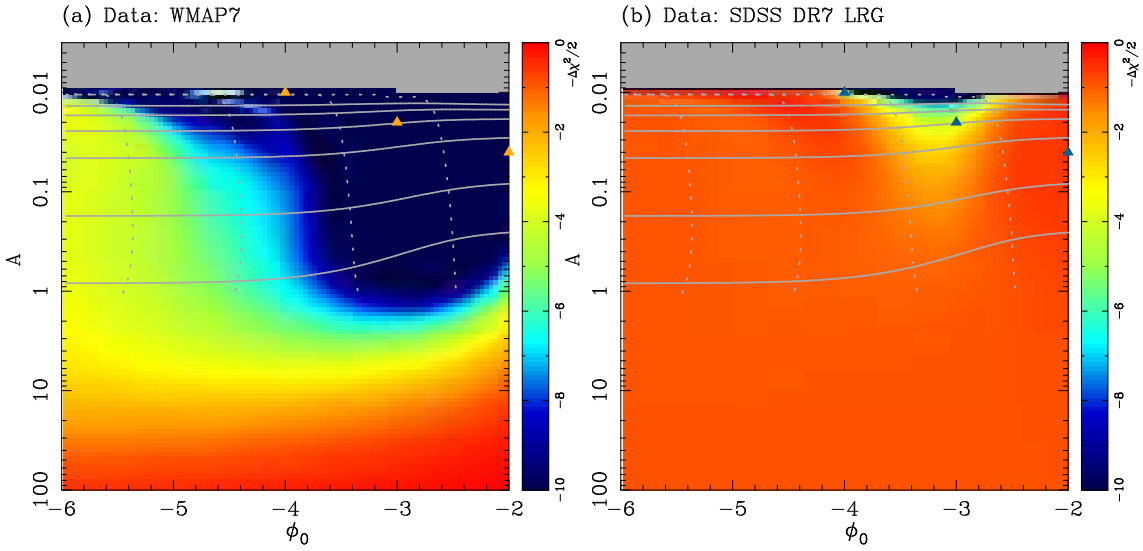

FIG. 4: Probability distributions of potential parameters, ϕ_0 and A, favored by (a) the WMAP 7-year data and (b) the SDSS DR7 LRG power spectrum. The gray region with $A \lesssim 0.01$ corresponds to the forbidden region where the permanent acceleration occurs. The relative logarithmic probability ($\Delta \ln P = -\Delta\chi^2/2$) decreases from red to dark blue. The dotted curves represent the epoch of EDE domination at maximum ($a = 10^{-6}$, 10^{-5}, 10^{-4}, 10^{-3} from left to right) while the solid curves indicate the strength of dark energy at maximum ($\Omega_\phi = 0.06$, 0.1, 0.2, 0.3, 0.4, 0.5 from bottom to top). Triangles indicate the potential parameters of three EDE models (EDE-1–3) chosen in the Markov chain Monte Carlo analysis (see Fig. 5 and Table I).

III. OBSERVATIONAL CONSTRAINTS ON EARLY EPISODICALLY DOMINATING DARK ENERGY MODEL

A. Observational signatures of scalar-field based EDE model

In order to see observational signatures of our scalar-field based EDE model, we consider both the scalar- and tensor-type perturbations in a system of multiple components for radiation, matter, and a minimally coupled scalar field without direct mutual interactions among the components. For this purpose, we modified the publicly available CAMB and CosmoMC packages [21, 22] by including the evolution of background and perturbation of the scalar field quantities.

Figure 3 shows the evolution of background densities and dark energy equation of state, baryonic matter density power spectrum, and CMB temperature and polarization power spectra in the EDE model with some chosen values of ϕ_0. Here the strength of the ephemeral domination has been fixed to $\Omega_\phi = 0.3$ by adjusting the potential parameter A. For smaller ϕ_0 the epoch of the ephemeral domination occurs earlier. We note that the dark energy component shows scaling behavior during the radiation and matter dominated era except for the transient domination period and that episodically dominating dark energy strongly affects the evolution of perturbations. Figure 3 implies that for the same episodic strength the EDE domination has weak observational effects if it occurs before the radiation-matter equality (the cases of $\phi_0 = -5$ and -4). However, the EDE domination near (or after) that epoch induces significant deviations from ΛCDM model prediction. For example, in the case of $\phi_0 = -3$ which corresponds to EDE domination near radiation-matter equality, we observe highly oscillatory features at small angular scales in the CMB temperature anisotropy and the strong deviation from ΛCDM model at all angular scales in the polarization power spectra. Though the effects are much weaker, the same is true in the case of $\phi_0 = -2$. Compared with the CMB anisotropy, however, the matter power spectrum is less sensitive to the presence of episodic domination of dark energy.

In the next two subsections, we explore the parameter constraints of the conventional cosmological parameters in the presence of episodic domination of dark energy using the recent CMB data together with other external data sets.

B. Constraints from WMAP data

First, we probe the overall ranges of potential parameters that are favored by CMB and large-scale structure data. Figure 4 shows probability distributions of the scalar field potential parameters obtained with the Wilkinson Microwave Anisotropy Probe (WMAP) 7-year data [23] and the Sloan Digital Sky Survey Data Release 7 Luminous Red Galaxies (SDSS DR7 LRG) power spectrum [24]. Here only the potential parameters, ϕ_0 and A, have been probed in a gridded space while other cos-

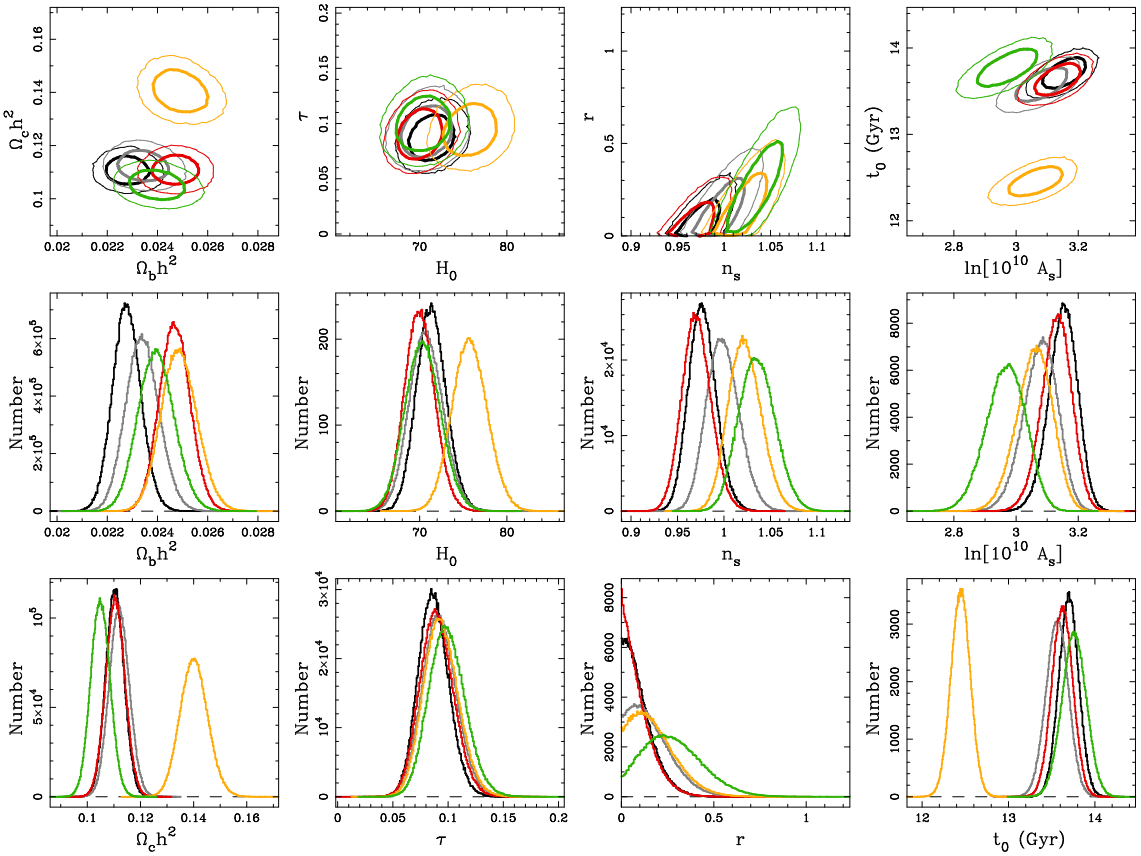

FIG. 5: Top: Two-dimensional likelihood contours favored by WMAP7+LRG+H_0 data sets for EDE-1 ($\phi_0 = -4$, $A = 0.01$; red), EDE-2 ($\phi_0 = -3$, $A = 0.02$; yellow), and EDE-3 ($\phi_0 = -2$, $A = 0.04$; green contours) models. For all models we set $\lambda = 10$. The 68.3% and 95.4% confidence limits are indicated by the thick and thin solid curves, respectively. The results for the SDE ($\phi_0 = -3$, $A = 100$; gray) and ΛCDM (black contours) models are shown for comparison. Middle and bottom: Marginalized one-dimensional likelihood distributions for each cosmological parameter.

mological parameters are fixed with the fiducial ΛCDM best-fit values (see Table 14 of [1]). The relative logarithmic probability is defined as $\Delta \ln P = -\Delta\chi^2/2 = -(\chi^2 - \chi^2_{\rm min})/2$, where $\chi^2_{\rm min}$ is the minimum chi-square determined within the area probed. It is shown that the epoch and strength of dark energy domination are controlled by ϕ_0 and A: the smaller ϕ_0 (A) gives the earlier (stronger) dark energy domination. The presence of EDE has a major effect on the CMB anisotropy after the radiation-dominated era ($a \gtrsim 10^{-4}$). On the other hand, the matter density perturbation is generally less sensitive to the EDE, being affected by only the strong EDE domination near the radiation-matter equality ($a \approx 10^{-4}$–10^{-3}). Therefore, as noted earlier, the parameter constraint are not much improved by adding the galaxy power spectrum. In this example, we directly use the galaxy power spectrum measured from the SDSS data. During the model constraining, we have effectively excluded the galaxy power spectrum information at scales $k > 0.1\ h{\rm Mpc}^{-1}$ where the nonlinear clustering dominates. The effect of bias parameter of galaxy clustering relative to the underlying dark matter distribution is taken into account by marginalizing over the overall amplitude of the galaxy power spectrum (see Sec. 3 of [24]). We have not used the SNIa data because it is sensitive only to the late-time acceleration of the universe and does not affect the behavior of our EDE models with a limited range of $\phi_0 \leq -2$.

In this example, the potential parameters with the larger value of ϕ_0 and the smaller value of A seem to be disfavored by the observational data. However, we will see later that such potential parameters (denoted as triangles in Fig. 4 as an example) can be favored by the current observations if different values of conventional cosmological parameters are chosen.

Next, we probe the conventional cosmological parameters in the presence of EDE component and compare the results with those in the ΛCDM model. To obtain the probability (likelihood) distributions for those parameters, we apply the Markov chain Monte Carlo (MCMC) method and randomly explore the parameter space that is favored by the recent astronomical observations. The MCMC method needs to make decisions whether it accepts or rejects a randomly chosen chain element via the probability function $P(\boldsymbol{\theta}|\mathbf{D}) \propto \exp(-\chi^2/2)$, where $\boldsymbol{\theta}$ denotes a vector containing free model parameters and $\mathbf{D}$

TABLE I: Mean and standard deviation (68.3% confidence limit) of cosmological parameters estimated from the marginalized one-dimensional likelihood distribution for best-fit ΛCDM, SDE, EDE models ($\lambda = 10$) constrained with the recent observational data sets (WMAP7+LRG+H_0). For tensor-to-scalar ratio r, the upper limit or the peak-location in the likelihood is presented.

Parameter	ΛCDM	SDE	EDE-1	EDE-2	EDE-3
(ϕ_0, A)		$(-3, 100)$	$(-4, 0.01)$	$(-3, 0.02)$	$(-2, 0.04)$
$100\Omega_b h^2$	2.281 ± 0.056	2.344 ± 0.066	2.473 ± 0.061	2.491 ± 0.071	2.399 ± 0.072
$\Omega_c h^2$	0.1106 ± 0.0035	0.1123 ± 0.0038	0.1108 ± 0.037	0.1404 ± 0.052	0.1052 ± 0.036
h	0.714 ± 0.017	0.709 ± 0.0019	0.701 ± 0.017	0.758 ± 0.020	0.705 ± 0.020
τ	0.088 ± 0.014	0.093 ± 0.015	0.091 ± 0.015	0.095 ± 0.016	0.100 ± 0.016
n_s	0.978 ± 0.015	1.000 ± 0.017	0.972 ± 0.016	1.024 ± 0.018	1.037 ± 0.019
r	< 0.128	< 0.199	< 0.109	< 0.225	$0.220^{+0.179}_{-0.132}$
$\ln[10^{10} A_s]$	3.153 ± 0.046	3.080 ± 0.055	3.132 ± 0.049	3.061 ± 0.058	2.970 ± 0.063
t_0 (Gyr)	13.70 ± 0.12	13.57 ± 0.13	13.63 ± 0.12	12.45 ± 0.11	13.77 ± 0.14

the data used, χ^2 the sum of individual chi-squares for CMB, large-scale structure data, Hubble constant, and so on. We use the modified version of CAMB/CosmoMC software that includes the evolution of minimally coupled scalar field to obtain the likelihood distribution of free parameters. A simple diagnostic has been used to test the convergence of MCMC chains (see Appendix B of Ref. [25]).

Depending on the epoch and strength of EDE domination, we consider three spatially flat models where the dark energy dominates at radiation era (EDE-1), near radiation-matter equality (EDE-2), and at early matter era (EDE-3) by fixing $(\phi_0, A) = (-4, 0.01)$, $(-3, 0.02)$, and $(-2, 0.04)$, respectively, and $\lambda = 10$. In each model, the value of A has been chosen so that we can obtain the chi-square between model and data that is similar to that of ΛCDM best-fit model. Thus, the free parameters are $\Omega_b h^2$, $\Omega_c h^2$, h, τ, n_s, r, and $\ln[10^{10} A_s]$, where Ω_b (Ω_c) is the baryon (CDM) density parameter at the current epoch, h is the normalized Hubble constant with $H_0 = 100h$ km s^{-1} Mpc^{-1}, τ is the reionization optical depth, n_s is the spectral index of the primordial scalar-type perturbation, r is the ratio of tensor- to scalar-type perturbations, and A_s is related to the amplitude of the primordial curvature perturbations by $A_s = k^3 P_{\mathcal{R}}(k)/(2\pi^2)$ at $k_0 = 0.002$ Mpc^{-1}. The running spectral index is not considered (see Ref. [1] for detailed descriptions of the parameters) [33]. In order to constrain the model parameters we use the CMB temperature and polarization power spectra measured from the WMAP 7-year data [23], the galaxy power spectrum measured from the SDSS DR7 LRG sample [24], and the recent measurement of the Hubble constant from the Hubble Space Telescope ($H_0 = 74.2 \pm 3.6$ km s^{-1} Mpc^{-1}; [26]). From here on we denote the combined data sets as WMAP7+LRG+H_0.

The results of parameter constraints obtained with the MCMC method are presented in Fig. 5, which shows two-dimensional likelihood contours and marginalized one-dimensional likelihood distributions of cosmological parameters favored by WMAP7+LRG+H_0 data sets for three EDE, SDE, ΛCDM models. Table I lists mean and 68.3% confidence limit of cosmological parameters estimated from the marginalized one-dimensional likelihood distributions. For tensor-to-scalar ratio r, however, we present the location of the peak with 68.3% (upper) limit in the likelihood distribution.

The parameter constraints for EDE-1 model are consistent with those for ΛCDM and SDE models, which implies that for our chosen strength of the episode the EDE domination at the early radiation era does not much affect the overall evolution of density perturbations. On the other hand, we notice significant deviations in the parameter constraints in EDE-2 and EDE-3 results. First, in the case of EDE-2, some cosmological parameters at the best-fit position significantly deviate from the ΛCDM likelihood distribution by over 3σ: compare the best-fit EDE-2 model parameters ($100\Omega_b h^2 = 2.491 \pm 0.071$, $\Omega_c h^2 = 0.1404 \pm 0.0052$, $n_s = 1.024 \pm 0.018$) with the ΛCDM ones ($100\Omega_b h^2 = 2.281 \pm 0.056$, $\Omega_c h^2 = 0.1106 \pm 0.0035$, $n_s = 0.978 \pm 0.015$). Interestingly, the EDE-2 model fits data better than ΛCDM model, that is, the minimum value of chi-square at the best-fit position in the EDE-2 model ($\chi^2_{\rm min}/2 = 3748.6$) is smaller than the ΛCDM value ($\chi^2_{\rm min}/2 = 3750.1$), and the derived cosmic age ($t_0 = 12.45 \pm 0.11$ Gyr) is quite smaller than that of ΛCDM model ($t_0 = 13.70 \pm 0.12$ Gyr). Secondly, the EDE-3 model prefers the larger spectral index and the positive tensor-to-scalar ratio ($n_s = 1.037 \pm 0.019$, $r = 0.22 \pm 0.16$), implying that the presence of early episodic dark energy at early matter era demands the existence of strong tensor-type perturbations unlike the best-fit ΛCDM model with r consistent with zero. In some sense, the large tensor-to-scalar ratio $r = 0.20^{+0.07}_{-0.05}$ from the recent B-mode polarization measurement of the BICEP2 experiment [27] can be mimicked by the transient behavior of dark energy, although such a large value of r is not allowed in the EDE model constrained by the

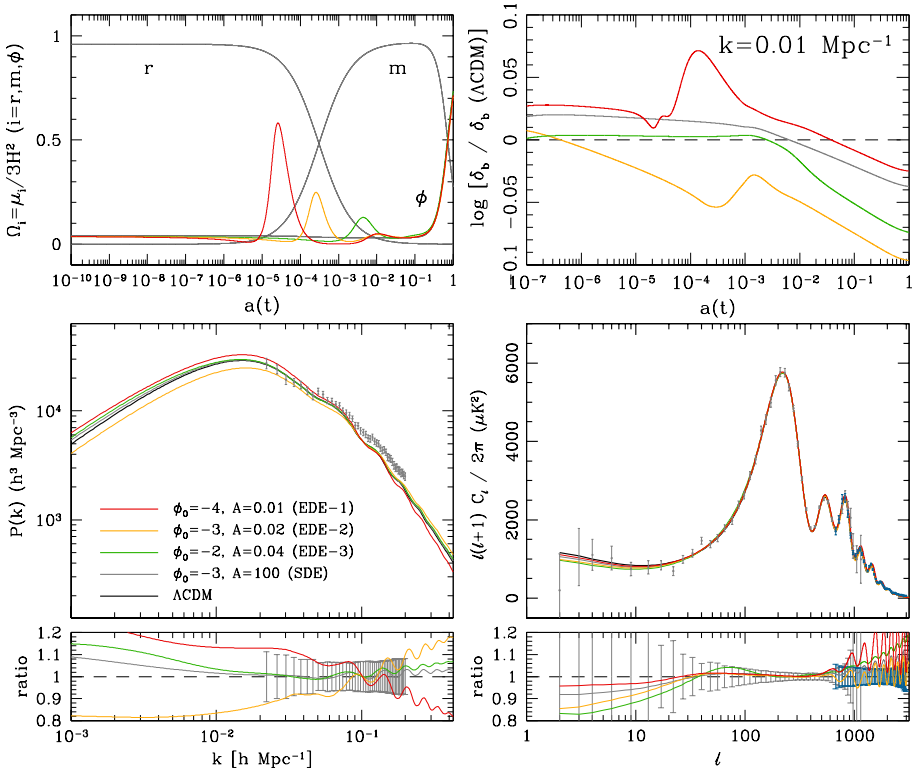

FIG. 6: Evolution of background density parameters (top-left) and baryon density perturbations ($\delta_b \equiv \delta\mu_b/\mu_b$ in the CDM-comoving gauge) at $k = 0.01$ Mpc^{-1} relative to the ΛCDM model (top-right), and baryonic matter and CMB anisotropy power spectra (sum of contributions from scalar- and tensor-type perturbations; bottom panels) for three best-fit EDE, ΛCDM, and SDE models, with the same color codes as in Fig. 5. For matter and CMB power spectra, recent measurements from SDSS DR7 LRG [24] and WMAP 7-year [1] data have been added (gray dots with error bars). In the ratio panels, we present the power ratio relative to the ΛCDM prediction together with the fractional error bars of the observational data including SPT data (at $\ell \gtrsim 600$; blue bars) [32].

Planck data (see next subsection).

Figure 6 shows the evolution of background and perturbation quantities, and the matter and CMB power spectra of the three best-fit EDE models. It should be noted that the CMB temperature power spectrum is the sum of contributions from the scalar- and tensor-type perturbations. The evolution of baryon density perturbations ($\delta_b = \delta\mu_b/\mu_b$ in the CDM-comoving gauge) relative to the ΛCDM model at comoving wavenumber $k = 0.01$ Mpc^{-1} shows that the growth of perturbation is affected by the episodic domination of dark energy. Here the initial amplitudes of baryon density perturbation are different among models because of the differently chosen best-fit initial power spectrum amplitude (A_s). The consequent EDE model power spectra, which are observationally indistinguishable with ΛCDM ones, suggests that the different parameter constraints with significant statistical deviations from the ΛCDM model can be obtained by introducing the alternative dark energy model (here with the early episodically dominating dark energy) even based on the same observational data.

The WMAP 9-year data [28] will provide parameter constraints a bit tighter than our WMAP 7-year result because the noise level of WMAP 9-year measurement decreases by a factor of $\sqrt{9/7} = 1.13$ compared with WMAP 7-year one without dramatic changes in systematic effects. We expect that even tighter constraints on model parameters are obtained if our EDE model is confronted to recent CMB data with higher precision at small angular scales, e.g., from the South Pole Telescope (SPT) [32] (compare EDE model's deviations relative to ΛCDM model with the size of SPT error bars in Fig. 6 bottom-right panel) and Planck (next subsection).

C. Constraints from Planck data

With the same numerical tools, we have explored the parameter constraints using the recent CMB data from the Planck satellite [2]. Due to the Planck's high precision up to small angular scales ($\ell \approx 3000$), even tighter constraints on model parameters are expected. The Planck data includes the CMB temperature anisotropy angular power spectrum, WMAP 9-year polarization data (WP) [28], and the cross-correlation between them [34]. We use the Planck data (CAMspec version 6.2) and run the modified CosmoMC software to obtain the likelihood distribution of cosmological parameters. As in the

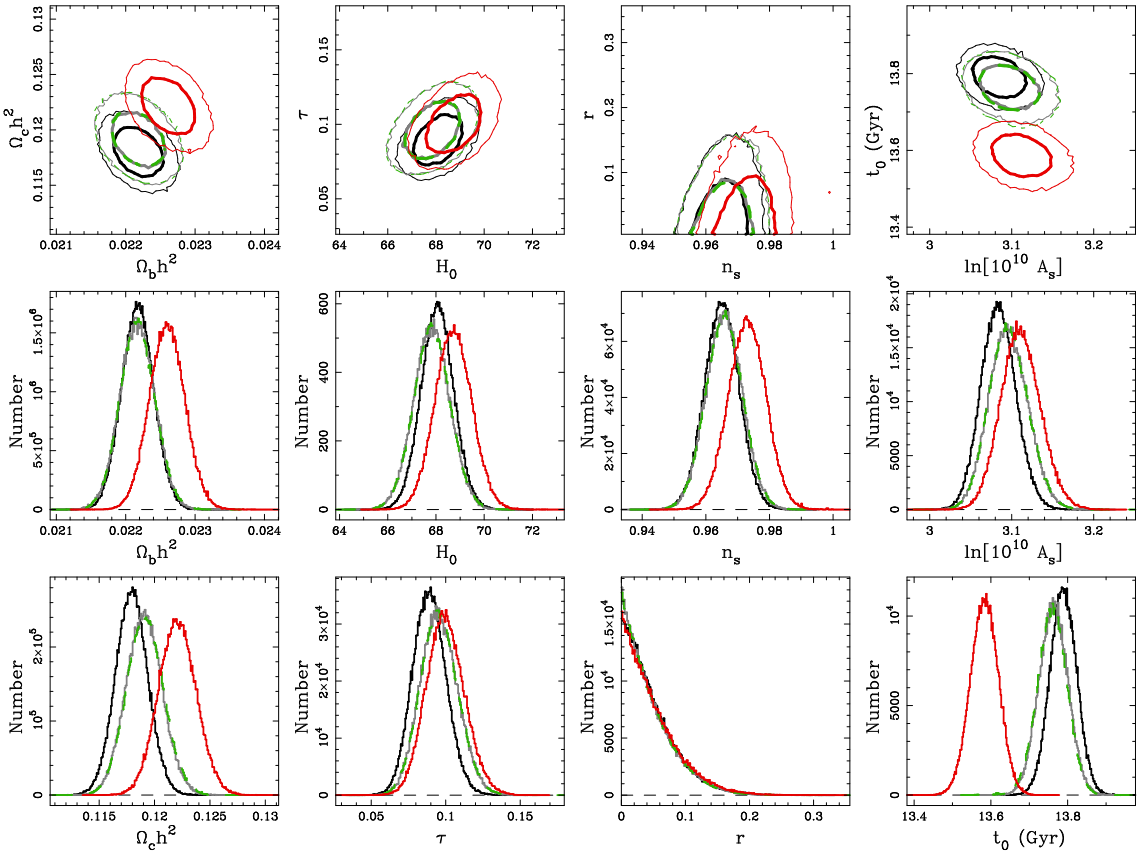

FIG. 7: Top: Two-dimensional likelihood contours favored by the recent observations (Planck+WP+BAO) for EDE-4 (with ϕ_0, A, λ as free parameters; green dashed) and EDE-5 ($\phi_0 = -5$, $A = 0.01$, $\lambda = 20$; red contours) models. The 68.3% and 95.4% confidence limits are indicated by the thick and thin solid curves, respectively. The results for the SDE (gray) and ΛCDM (black contours) models are shown for comparison. Middle and bottom: Marginalized one-dimensional likelihood distributions for each cosmological parameter.

TABLE II: Mean and standard deviation (68.3% confidence limit) in the marginalized one-dimensional likelihood distribution for best-fit ΛCDM, SDE, EDE models constrained with the recent observational data sets (Planck+WP+BAO). For SDE model, λ is a free parameter. For EDE-4 model, free potential parameters are λ, ϕ_0, and A. For tensor-to-scalar ratio r, the upper limit is presented.

Parameter	ΛCDM	SDE ($\phi_0 = -3, A = 100$)	EDE-4	EDE-5 ($\lambda = 20, \phi_0 = -1.5, A = 0.01$)
$100\Omega_b h^2$	2.219 ± 0.023	2.218 ± 0.025	2.218 ± 0.025	2.261 ± 0.025
$\Omega_c h^2$	0.1180 ± 0.0015	0.1192 ± 0.0016	0.1192 ± 0.0017	0.1222 ± 0.0017
h	0.6810 ± 0.0068	0.6786 ± 0.0075	0.6787 ± 0.0076	0.6876 ± 0.0076
τ	0.090 ± 0.011	0.096 ± 0.013	0.096 ± 0.013	0.101 ± 0.013
n_s	0.9653 ± 0.0054	0.9660 ± 0.0057	0.9660 ± 0.0058	0.9733 ± 0.0059
r	< 0.054	< 0.051	< 0.054	< 0.057
$\ln[10^{10} A_s]$	3.085 ± 0.021	3.097 ± 0.024	3.098 ± 0.024	3.112 ± 0.024
t_0 (Gyr)	13.790 ± 0.035	13.765 ± 0.038	13.761 ± 0.039	13.585 ± 0.036

Planck team's analysis, effects of unresolved foregrounds, calibration, and beam uncertainties have been considered and the related parameters have been marginalized over [2]. The pivot scale for the initial power spectrum amplitude has been set to $k = 0.05$ Mpc^{-1}. As the large-scale structure data, we use the BAO measurements obtained from the Six-Degree-Field Galaxy Survey [29], the SDSS DR 7 [30], and Baryon Oscillation Spectroscopic Survey DR 9 [31].

With the combined data sets (denoted as

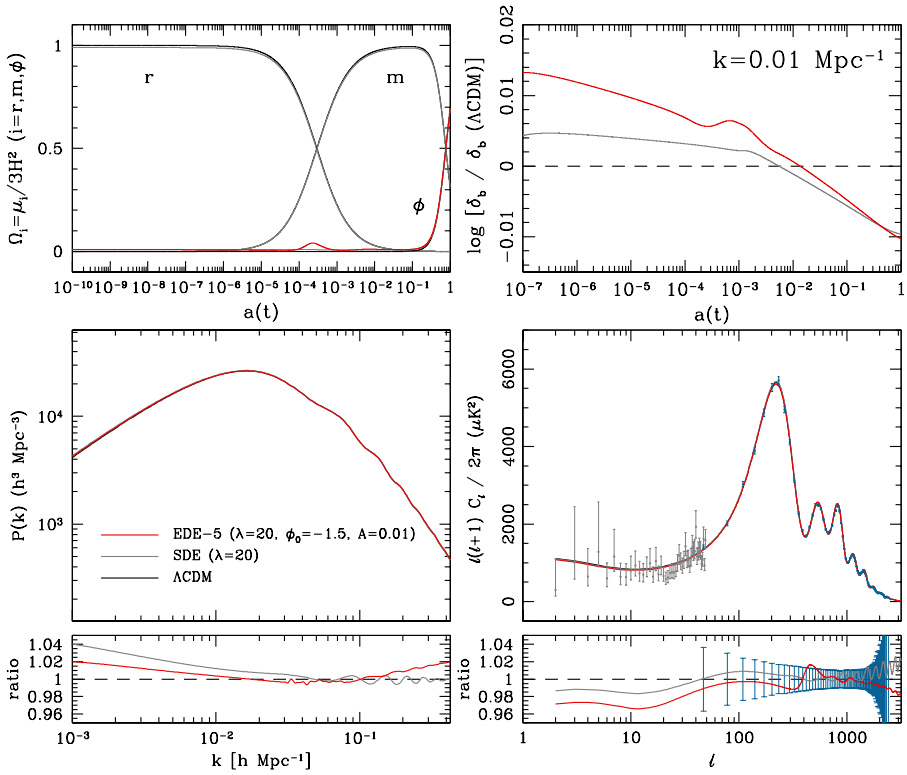

FIG. 8: Evolution of background density parameters (top-left) and baryon density perturbations ($\delta_b \equiv \delta\mu_b/\mu_b$ in the CDM-comoving gauge) at $k = 0.01$ Mpc^{-1} relative to the ΛCDM model (top-right), and baryonic matter and CMB anisotropy power spectra (bottom panels) for the EDE-5, SDE, and ΛCDM models best-fitting Planck+WP+BAO data sets, with the same color codes as in Fig. 7. Note that the CMB temperature power spectrum is the sum of contributions from the scalar- and tensor-type perturbations. For CMB temperature power spectrum, the recent measurement from Planck data [2] has been added (gray and blue dots with error bars). In the ratio panels, we present the power ratio relative to the ΛCDM prediction together with the fractional error bars of the observational data (only for Planck CMB angular power spectrum at small angular scales).

Planck+WP+BAO), we have constrained the parameter space of spatially flat ΛCDM, SDE, and EDE models that are favored by the observations. The results are summarized in Fig. 7 and Table II.

For SDE model, we have set λ as a free parameter to constrain the initial level of dark energy allowed at the early epoch. The allowed range for this parameter is $\lambda > 17.9$, which corresponds to the level of early dark energy $\Omega_e \lesssim 0.012$ (95.4% confidence limit). This result is similar to the recent constraint on the fluid-based EDE density parameter obtained from the Planck observation [2]. When Planck+WP+BAO data sets are used, the parameter constraints of SDE model are very similar to those of ΛCDM model. The chi-square value at the best-fit position is $\chi^2_{\rm min}/2 = 4909.3$ for SDE and 4908.1 for ΛCDM model. The SDE model prefers slightly larger values of $\Omega_c h^2$, τ, and $\ln[10^{10} A_s]$ and smaller value of h and t_0 (age) than ΛCDM model. The estimated parameters of both models are consistent within 1σ uncertainty, with small differences less than one percent.

For EDE models, we have considered two cases. In the first case, the observational data sets have been compared with an EDE model where the potential parameters λ, A, ϕ_0 are all freely varied together with the conventional cosmological parameters, but with flat priors, $10 \leq \lambda \leq 25$, $-2.3 \leq \log_{10} A \leq 1$, and $-5 \leq \phi_0 \leq -1$ (hereafter EDE-4). With the Planck+WP+BAO data, the potential parameters in the direction to the upper (lower) bound of λ and A (ϕ_0) are preferred [35], and the resulting constraints on the conventional cosmological parameters are essentially the same as those in the SDE case, with $\chi^2_{\rm min}/2 = 4909.4$ (see Table II). The parameter constraint results above suggest that the Planck+WP+BAO data sets strongly favor the ΛCDM model than the scalar-field based EDE model.

Although the Planck data provides a really tight constraint on the ΛCDM model, as a second case we consider a particular EDE model in which the early episodic domination of dark energy occurs near the radiation-matter equality (hereafter EDE-5). We have designed this model by setting $A = 0.01$, $\phi_0 = -1.5$ for $\lambda = 20$ to make the dark energy density have the maximum strength $\Omega_\phi = 0.04$ around the radiation-matter equality. The choice of $\lambda = 20$ is to fix the level of early dark energy, $\Omega_{\phi,i} = 0.01$, based on the fluid-based EDE constraint from Planck data [2]. The results are presented in Fig. 7

and Table II.

Figure 8 shows the evolution of background and perturbation quantities, and the matter and CMB power spectra of the best-fit ΛCDM, SDE (with $\lambda = 20$ fixed), and EDE-5 ($\phi_0 = -1.5$, $A = 0.01$, $\lambda = 20$) models. The best-fit designed EDE model has a small bump in the dark energy density parameter with the maximum at $a = 2.3 \times 10^{-4}$ or redshift $z = 4350$ (top-left panel). The evolution of baryon density perturbation behaves in a similar way to that of EDE-2 model, but now with the smaller difference from ΛCDM model. The designed EDE model gives a poorer fit, with the minimum chi-square value ($\chi^2_{\rm min}/2 = 4911.1$) larger than ΛCDM model. However, in the matter and CMB power spectra, the deviation of the best-fit EDE model from ΛCDM one is small, showing only a few % difference at all scales (see Fig. 8 bottom panels showing the power spectrum ratio relative to ΛCDM model). The EDE model predictions are consistent with observational data within uncertainties, except for the slightly larger amplitude of CMB temperature power spectrum around the second acoustic peak, which is the primary reason for the deviation from ΛCDM model.

The deviation of parameter constraints between this model (EDE-5) and ΛCDM is still quite small as expected, but with noticeable differences. We note the similar behavior of parameter deviation as seen in the case of EDE-2 model (constrained with WMAP7+LRG+H_0 data). For example, the EDE-5 model favors the baryon (CDM) density that is 1.9% (3.6%) higher than the ΛCDM best-fit value, with a statistical deviation by 1.8σ (2.8σ). Besides, the derived cosmic age ($t_0 = 13.585 \pm 0.036$ Gyr) is smaller than the ΛCDM best-fit value ($t_0 = 13.790 \pm 0.035$ Gyr) with 1.5% difference (deviating from ΛCDM model by 5.8σ). Such deviations mentioned above become smaller as we choose the weaker episodic domination of dark energy in our EDE model.

Considering all the cases of ΛCDM, SDE and EDE models constrained with the Planck data, we found that the Planck data strongly favors the ΛCDM model and only a limited amount of dark energy with episodic nature is allowed. Although the statistical deviation from ΛCDM model is small, our results still imply that a different parameter estimation with some deviations from the ΛCDM model can be obtained based on the same observational data by introducing the ephemerally dominating dark energy at early epoch.

IV. SUMMARY AND CONCLUSION

In this paper, we investigate the observational effects of early episodically dominating dark energy based on a minimally coupled scalar field with the Albrecht-Skordis potential. Our results show that the episodic domination of the dark energy component can affect the cosmological parameter constraints significantly, compared with the conventional estimation based on the ΛCDM model. For the WMAP data, we found that the EDE dominating after the radiation era (EDE-2, EDE-3) affects the growth of density perturbations (Fig. 6), consequently modifying the observationally favored parameter space, compared with the ΛCDM model (Fig. 5); one can make a model that prefers the shorter cosmic age (EDE-2) or the existence of tensor-type perturbation (EDE-3).

For the Planck data, the effect of early dark energy with episodic nature should be sufficiently suppressed to be consistent with observational data (EDE-4). However, we note the similar trends as seen in the EDE models constrained with WMAP data (Fig. 7). In the presence of transiently dominating dark energy at the early epoch, the estimated cosmological parameters can deviate from the currently known ΛCDM-based parameters with the percent level difference (EDE-5; Fig. 8).

We note that this interesting phenomenon is not seen in the case of the conventional dark energy model where the estimated cosmological parameters are very similar to ΛCDM parameters [1]. Our model can be considered as an example where alternative cosmological parameter estimations are allowed based on the same observations even in Einstein's gravity.

Appendix: Initial conditions for background evolution of EDE models

Here we present initial conditions for the background evolution of several EDE models considered in this paper. It should be noted that all the scalar field parameters and variables are expressed under the unit where $c \equiv 1$ and $8\pi G \equiv 1$. Besides, in the numerical calculation, the potential parameters V_0 and V_1 in Eq. (1) are expressed in unit of H_0^2, that is, $\hat{V}_0 = V_0/H_0^2$ and $\hat{V}_1 = V_1/H_0^2$. We have set $\hat{V}_0 \equiv 1$ and $\beta = 0$. Table III lists scaling initial conditions of background scalar field variables (ϕ_i, ϕ_i') at the initial epoch $a_i = 10^{-10}$, together with potential parameters of EDE models considered in Figs. 1, 3, 6, and 8. In Fig. 1, we assume the conventional cosmological parameters as those of spatially flat ΛCDM model from the WMAP 7-year result ([23]; $\Omega_b h^2 = 0.02260$, $\Omega_c h^2 = 0.1123$, $h = 0.704$, $T_0 = 2.725$ K, $N_\nu = 3.04$ [number of species of massless neutrinos]), while in Fig. 3, as those from the Planck result ([2]; $\Omega_b h^2 = 0.022161$, $\Omega_c h^2 = 0.11889$, $h = 0.6777$, $T_0 = 2.7255$ K, $N_\nu = 3.046$).

Acknowledgments

C.G.P. was supported by Basic Science Research Program through the National Research Foundation of Korea (NRF) funded by the Ministry of Science, ICT and Future Planning (No. 2013R1A1A1011107) and was partly supported by research funds of Chonbuk National University in 2012. J.H. was supported by Basic Science Research Program through the NRF of Korea

TABLE III: Scaling initial conditions of scalar field variables and potential parameters of EDE models.

Figure	Model	λ	ϕ_0	A	$\hat{V}_1$	ϕ_i	ϕ_i'
Fig. 1	SDE	10	-4	100	2.14417	-7.48116	0.397531
	EDE	10	-4	0.01	2.14134	-7.68262	0.379410
Fig. 3	SDE	10	-3	100	2.03666	-7.48180	0.397036
	EDE	10	-5	0.0187	2.03398	-7.74537	0.372901
	EDE	10	-4	0.0183	2.03309	-7.68996	0.379460
	EDE	10	-3	0.0162	2.03186	-7.64613	0.383504
	EDE	10	-2	0.0148	2.03253	-7.60993	0.386237
Fig. 6	SDE	10	-3	100	2.13829	-7.47420	0.397040
	EDE-1	10	-4	0.01	2.10625	-7.68552	0.379425
	EDE-2	10	-3	0.02	2.07960	-7.62556	0.383436
	EDE-3	10	-2	0.04	2.15929	-7.60357	0.386232
Fig. 8	SDE	20	-3	100	2.05858	-3.67975	0.199865
	EDE-5	20	-1.5	0.01	2.07378	-3.82015	0.191751

funded by the Ministry of Science, ICT and future Planning (No. 2013R1A1A2058205). H.N. was supported by NRF of Korea funded by the Korean Government (No. 2012R1A1A2038497).

[1] E. Komatsu, et al. Astrophys. J. Suppl. Ser. **192**, 18 (2011).
[2] P.A.R. Ade *et al.* [Planck Collaboration], arXiv:1303.5076 [astro-ph.CO].
[3] R. Laureijs *et al.* arXiv:1110.3193v1 [astro-ph.CO]; L. Amendola *et al.* [Euclid Theory Working Group Collaboration], Living Rev. Rel. **16** (2013) 6 [arXiv:1206.1225 [astro-ph.CO]].
[4] C.-G. Park, J. Hwang, J. Lee, H. Noh, Phys. Rev. Lett. **103**, 151303 (2009).
[5] M. Doran and G. Robbers, J. Cosmol. Astropart. Phys. **06**, 026 (2006).
[6] J.-Q. Xia and M. Viel, J. Cosmol. Astropart. Phys. **04**, 002 (2009).
[7] E. Calabrese, R. de Putter, D. Huterer, E.V. Linder, and A. Melchiorri, Phys. Rev. D **83**, 023011 (2011); E. Calabrese, D. Huterer, E.V. Linder, A. Melchiorri, and L. Pagano, Phys. Rev. D **83**, 123504 (2011); E. Calabrese, E. Menegoni, C.J.A.P. Martins, A. Melchiorri, and G. Rocha, Phys. Rev. D **84**, 023518 (2011).
[8] S. Joudaki and M. Kaplinghat, arXiv:1106.0299v2. S. Joudaki and M. Kaplinghat, Phys. Rev. D **86**, 023526 (2012) [arXiv:1106.0299 [astro-ph.CO]].
[9] U. Alam, Z. Lukić, and S. Bhattacharya, Astrophys. J. **727**, 87 (2011).
[10] C.L. Reichardt, R. de Putter, O. Zahn, and Z. Hou, Astrophys. J. **749**, L9 (2012).
[11] S. Joudaki, Phys. Rev. D 87, 083523 (2013).
[12] X.-m. Chen, Y. Gong and E.N. Saridakis, Int. J. Theor. Phys. **53** (2014) 469 [arXiv:1111.6743 [astro-ph.CO]]; C. Zuñiga Vargas, W.S. Hipólito-Ricaldi, and W. Zimdahl, J. Cosmol. Astropart. Phys. **04**, 032 (2012); R.-G. Cai, and Z.-L. Tuo, Phys. Lett. B **706**, 116 (2011); A.C.C. Guimarães, and J.A.S. Lima, Class. Quantum Grav. **28**, 125026 (2011).
[13] D. Blais, and D. Polarski, Phys. Rev. D **70**, 084008 (2004).
[14] A. Albrecht and C. Skordis, Phys. Rev. Lett. **84**, 2076 (2000); C. Skordis and A. Albrecht, Phys. Rev. D **66**, 043523 (2002).
[15] J.D. Barrow, R. Bean, and J. Magueijo, Mon. Not. R. Astron. Soc. **316**, L41 (2000).
[16] R. Bean, S.H. Hansen, and A. Melchiorri, Phys. Rev. D **64**, 103508 (2001).
[17] M. Barnard, A. Abrahamse, A. Albrecht, B. Bozek, and M. Yashar, Phys. Rev. D **77**, 103502 (2008).
[18] J.M. Fedrow and K. Griest, J. Cosmol. Astropart. Phys. **01**, 004 (2014) [arXiv:1309.0849 [astro-ph.CO]].
[19] J. Hwang and H. Noh, Phys. Rev. D **64**, 103509 (2001).
[20] J. Hwang and H. Noh, Phys. Rev. D **65**, 023512 (2001).
[21] A. Lewis and A. Lasenby, Astrophys. J. **513**, 1 (1999); A. Lewis, A. Challinor, and A. Lasenby, Astrophys. J. **538**, 473 (2000).
[22] A. Lewis, and S. Bridle, Phys. Rev. D **66**, 103511 (2002).
[23] D. Larson, J. Dunkley, G. Hinshaw, et al. Astrophys. J. Suppl. Ser. **192**, 16 (2011).
[24] B.A. Reid, W.J. Percival, D.J. Eisenstein, L. Verde, D.N. Spergel, R.A. Skibba, N.A. Bahcall and T. Budavari *et al.*, Mon. Not. Roy. Astron. Soc. **404**, 60 (2010).
[25] A. Abrahamse, A. Albrecht, M. Barnard, and B. Bozek, Phys. Rev. D **77**, 103503 (2008).
[26] A.G. Riess, L. Macri, S. Casertano, et al. Astrophys. J. **699**, 539 (2009).
[27] P.A.R. Ade *et al.* [BICEP2 Collaboration], Phys. Rev. Lett. **112**, 241101 (2014) [arXiv:1403.3985 [astro-ph.CO]].

[28] G. Hinshaw, D. Larson, E. Komatsu, et al. Astrophys. J. Suppl. , 208, 19 (2013)

[29] F. Beutler, C. Blake, M. Colless, D.H. Jones, L. Staveley-Smith, L. Campbell, Q. Parker and W. Saunders et al. Mon. Not. Roy. Astron. Soc. 416, 3017 (2011) [arXiv:1106.3366 [astro-ph.CO]].

[30] N. Padmanabhan, X. Xu, D.J. Eisenstein, R. Scalzo, A.J. Cuesta, K.T. Mehta and E. Kazin, Mon. Not. Roy. Astron. Soc. 427, 2132 (2012) [arXiv:1202.0090 [astro-ph.CO]].

[31] L. Anderson, E. Aubourg, S. Bailey, D. Bizyaev, M. Blanton, A.S. Bolton, J. Brinkmann and J.R. Brownstein et al., Mon. Not. Roy. Astron. Soc. 427, 3435 (2013) [arXiv:1203.6594 [astro-ph.CO]].

[32] R. Keisler, C.L. Reichardt, K.A. Aird, B.A. Benson, L.E. Bleem, J.E. Carlstrom, C.L. Chang and H.M. Cho *et al.*, Astrophys. J. **743**, 28 (2011).

[33] We choose the flat priors for the free parameters as $\Omega_b h^2 = [0.005, 0.100]$, $\Omega_c h^2 = [0.01, 0.99]$, $h = [0.4, 1.0]$, $\tau = [0.01, 0.80]$, $n_s = [0.5, 1.5]$, $r = [0, 2]$, $\ln(10^{10} A_s) = [2.7, 4.0]$.

[34] Based on observations obtained with Planck (http://www.esa.int/Planck), an ESA science mission with instruments and contributions directly funded by ESA Member States, NASA, and Canada.

[35] Within the flat priors, the allowed ranges of potential parameters are $\lambda > 18.2$, $\phi_0 < -1.62$, and $\log_{10} A > -2.11$ (95.4% confidence limits).